

High spatial resolution mapping of aerosol composition and sources in Oakland, California using mobile aerosol mass spectrometry

Shah et al.

5

Correspondence to: Albert A. Presto (apresto@andrew.cmu.edu)

A1 Accounting for temporal trends

Over the course of mobile sampling, the urban background air quality can have daily and diurnal variations due to meteorological changes. These variations can be accounted for with the help of concurrent stationary measurements performed at an urban background location, provided this background location is not in close proximity (≤ 50 m) of a major emission source (e.g., a street with > 3000 daily vehicles, construction sites, industrial emissions, etc; Hoek et al., 2002; Van den Bossche et al., 2015). Further, different meteorological conditions (temperature, relative humidity, solar irradiation) influence individual components of particulate matter differently (e.g., the gas-particle partitioning of NO_3^- , SO_4^{2-} and OA have different sensitivities to temperature; more irradiation can indirectly result in more secondary OA). Ideally, the temporal correction of mobile measurements of a particular PM component would be performed using background measurements of that individual component performed in the same manner. Thus, mobile AMS measurements should ideally be corrected using concurrent stationary AMS measurements (Mohr et al., 2015).

We did not perform concurrent stationary AMS measurements in Oakland in this campaign. Stationary measurements of criteria pollutants (CO , NO_x , $\text{PM}_{2.5}$, etc.) were made by a regulatory monitor operated by the Bay Area air quality management district. However, this monitor was located in a parking lot within ~ 30 m of a major street ($> 20,000$ vehicles daily; Knoderer et al., 2016). Due to this, we did not use this monitor as an indicator of diurnal variations in urban background. Instead, we assumed that by shuffling the order of visiting each polygon within the sampling domain, repeated measurements at a given point in space were well-balanced in time. We validated this assumption by running the timestamps of our data through the spatial aggregation routine described earlier. The resulting map (Figure S1) confirms that the measurements in this study were indeed well-balanced in space and time. Further, diurnal variations in meteorological factors had a consistent pattern on all days of this campaign (Figure S2), hence by balancing our samples in space and time, we assume that the effects of diurnal variations in urban background are nullified upon aggregation of data from multiple days.

Figure S2 shows that daily variations in meteorological factors is typically larger and sporadic relative to diurnal variations. To account for the possible effect of these daily variations on urban background, we tested a daily multiplicative correction factor to our mobile measurements based on stationary measurements of $\text{PM}_{2.5}$ at the regulatory site.

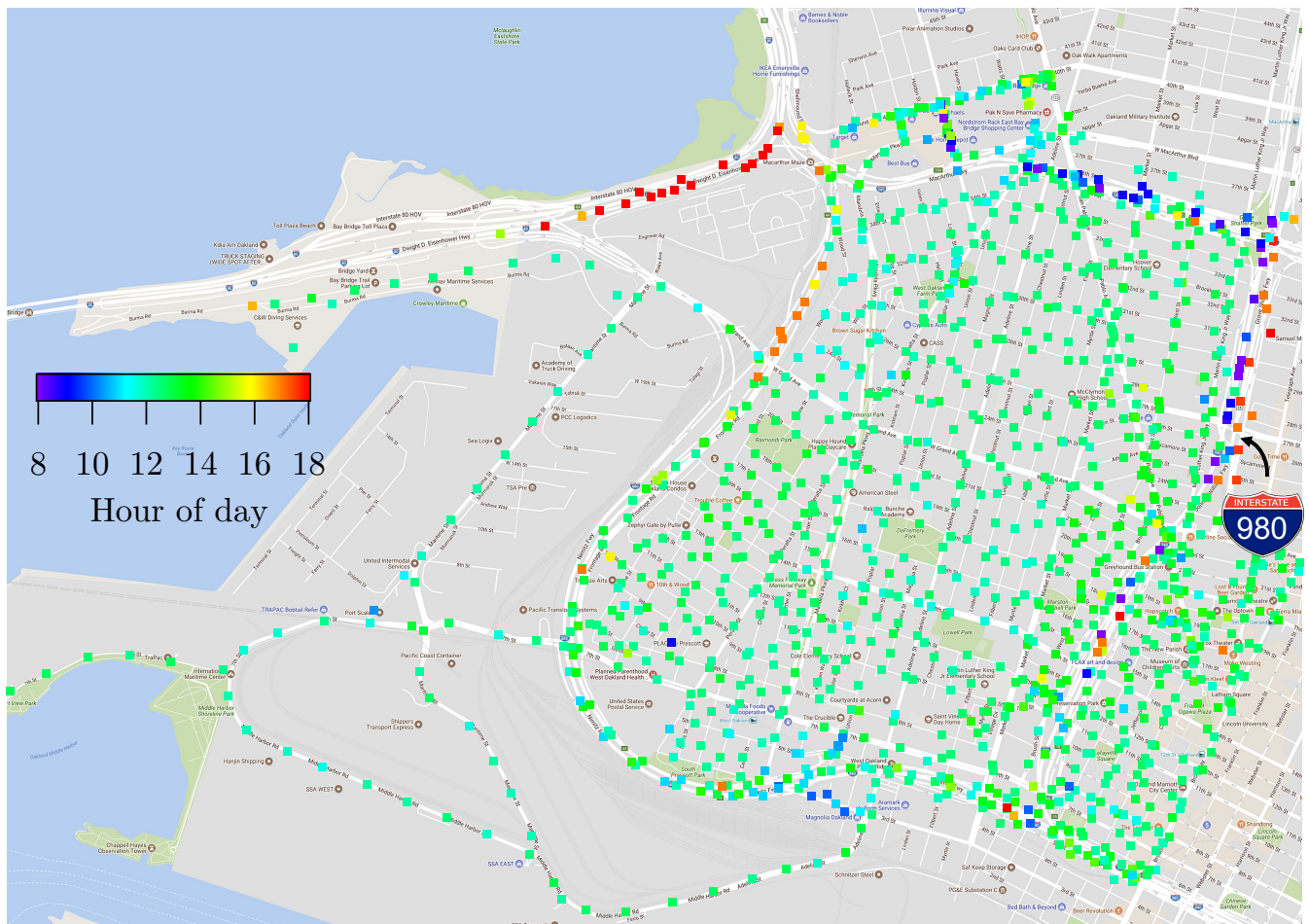


Figure S1. Spatially aggregated timestamp of all AMS measurements. Typically, drives were performed from 0800 to 1800 hours. If all parts of the domain were sampled randomly everyday, the average of all measurement timestamps should ideally occur at 1300 hours. This figure shows that this ideality was indeed realized in this campaign and that we balanced our measurements in space and time reasonably well. On most days, we used the south- and north-bound lanes of Interstate 980 to enter and exit the domain at 0800 and 1800 hours, respectively. As a result, there is a temporal bias in sampling this highway, as shown by the figure.

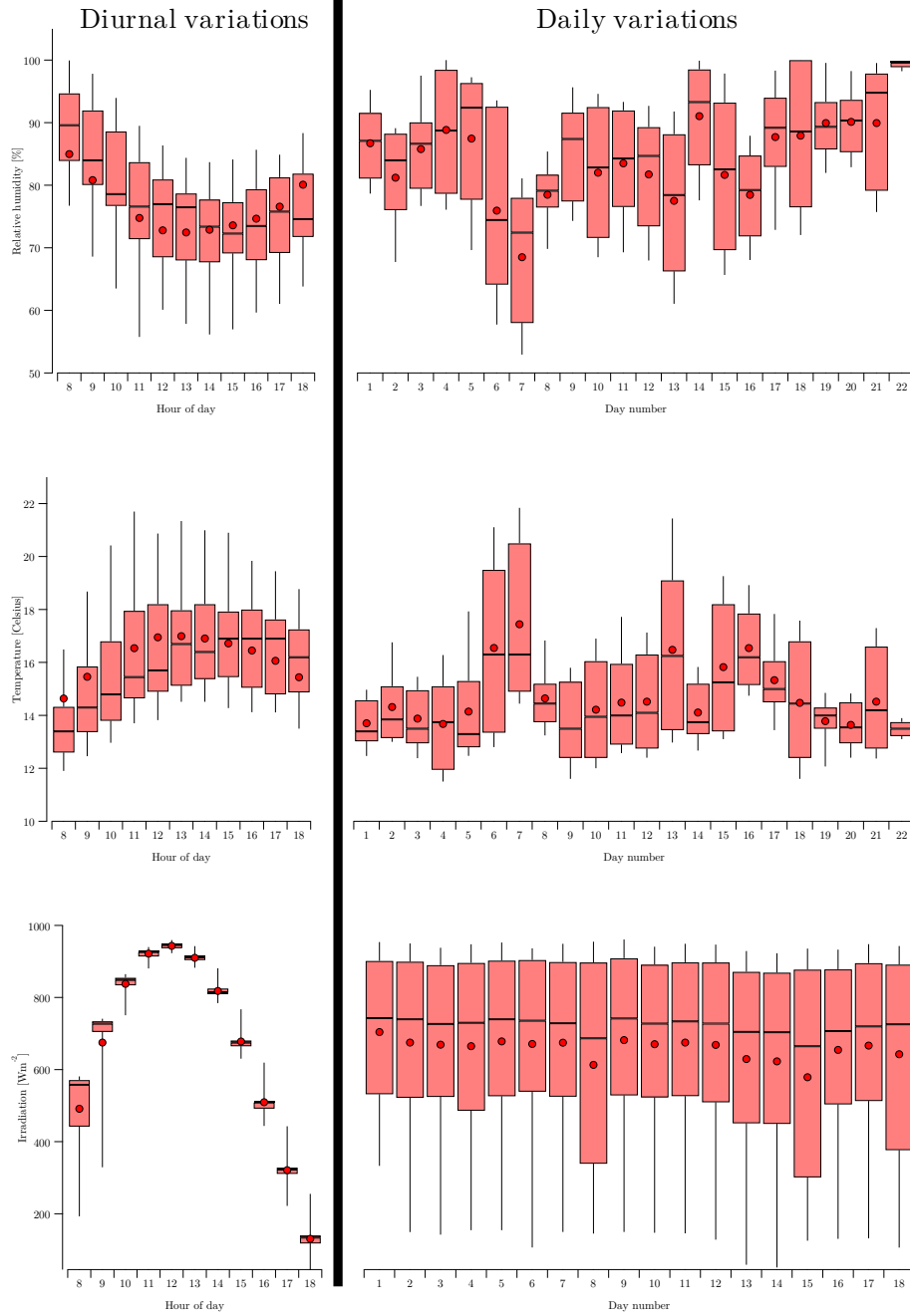


Figure S2. Diurnal and daily variations in meteorological factors in Oakland during the sampling period. Diurnal variations have a consistent pattern that repeats everyday. By comparison, daily variations have more sporadic variations.

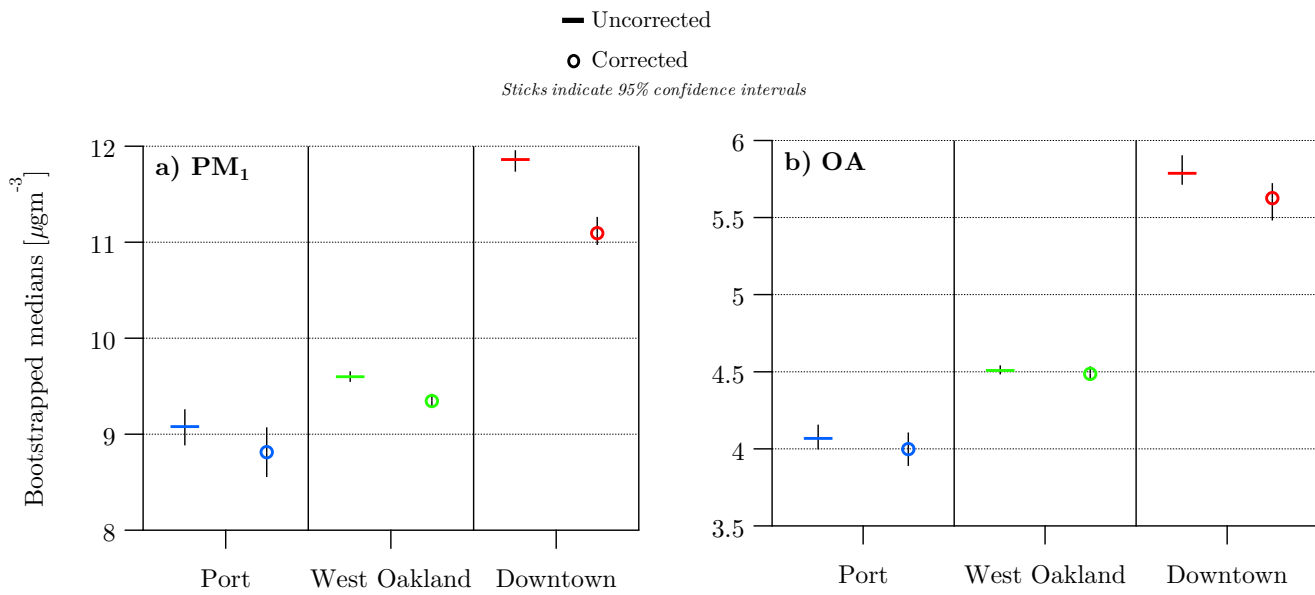


Figure S3. Effect of applying a daily correction factor to mobile measurements of a) PM₁ and b) OA. The 95% confidence intervals are achieved from bootstrapping and represent the difference between the 5th and 95th percentiles of the bootstrapped medians. Each day's correction factor is calculated as $CF_i = \frac{C_i}{C_{campaign}}$, where C_i is the median PM_{2.5} concentration measured on the i^{th} day of the campaign, and $C_{campaign}$ is the median PM_{2.5} concentration measured on all days of the campaign. Stationary PM_{2.5} measurements were made by the regulatory monitor in West Oakland (Knoderer et al., 2016). Since we typically drove everyday from 8 AM to 6 PM, we only used stationary data from this daily time period.

A2 Bootstrapping analysis

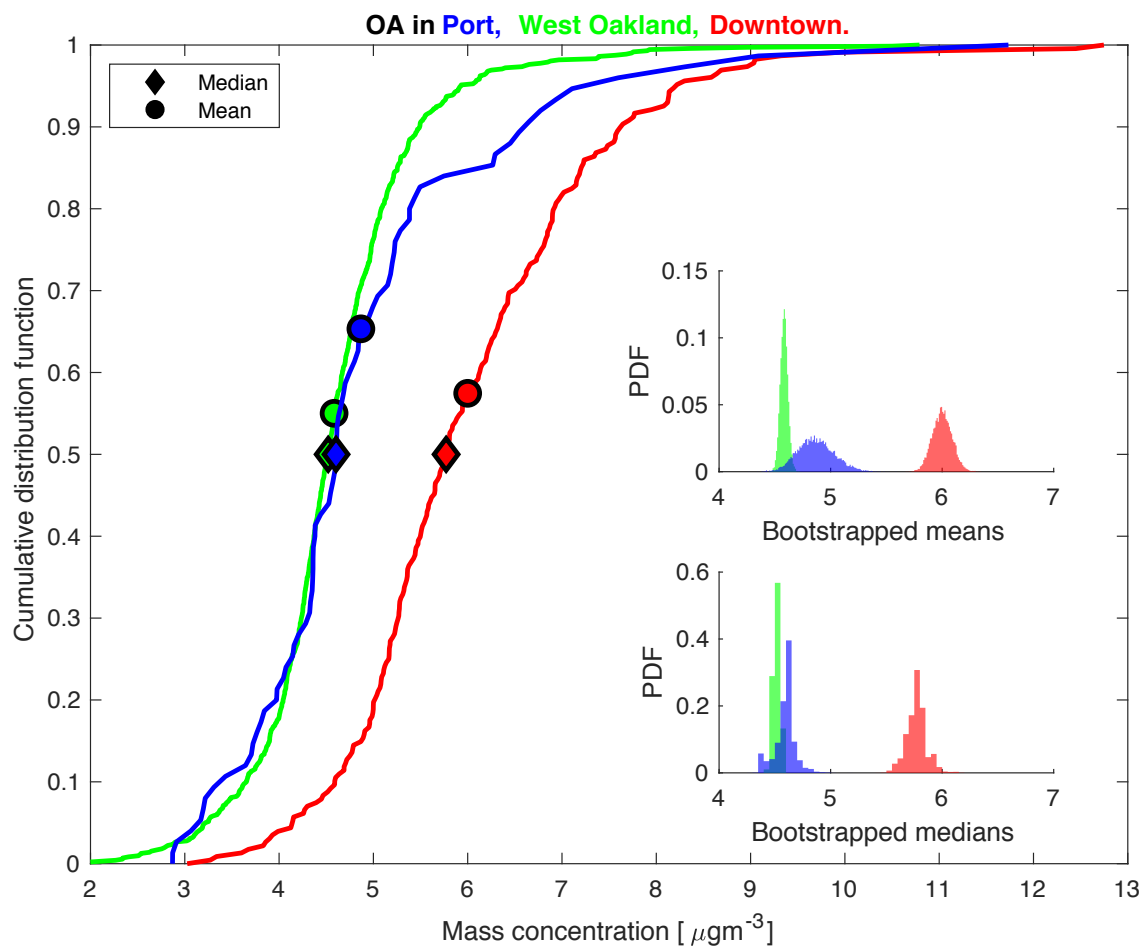


Figure S4. Polygon-specific cumulative distribution function (CDF) curves of spatially-aggregated OA concentrations. *Insets:* Probability distribution function (PDF) histograms for central tendency statistics (mean and median) of synthetic datasets created using bootstrap resampling. The PDF histogram for bootstrapped medians is shown with a coarser bin-width to guide the eye better. The abscissae on the insets have the same units as the parent abscissa, but with a zoomed-in scale.

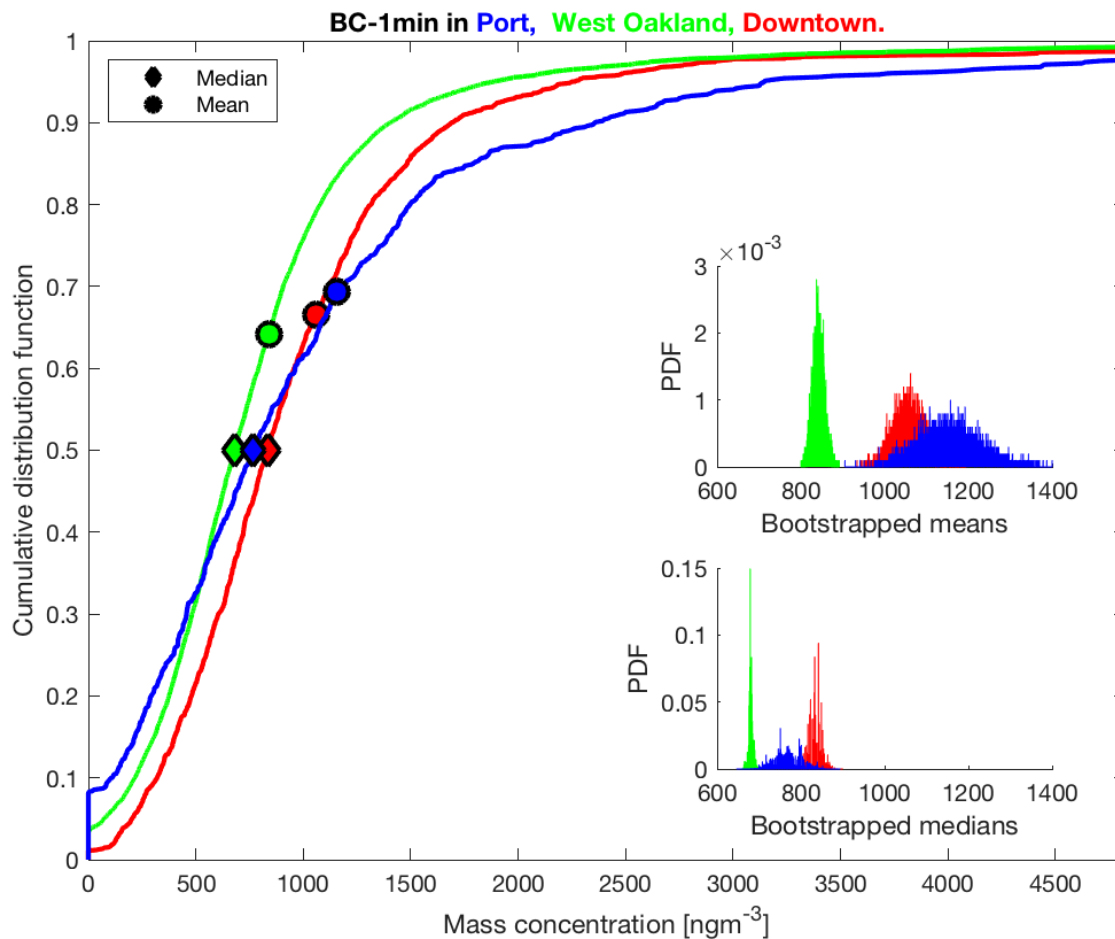


Figure S5. Polygon-specific cumulative distribution function (CDF) curves of black carbon (BC) concentrations. *Insets:* Probability distribution function (PDF) histograms for central tendency statistics (mean and median) of synthetic datasets created using bootstrap resampling of raw data. The PDF histograms are shown with a coarser bin-width to guide the eye better. The abscissae on the insets have the same units as the parent abscissa, but with a zoomed-in scale.

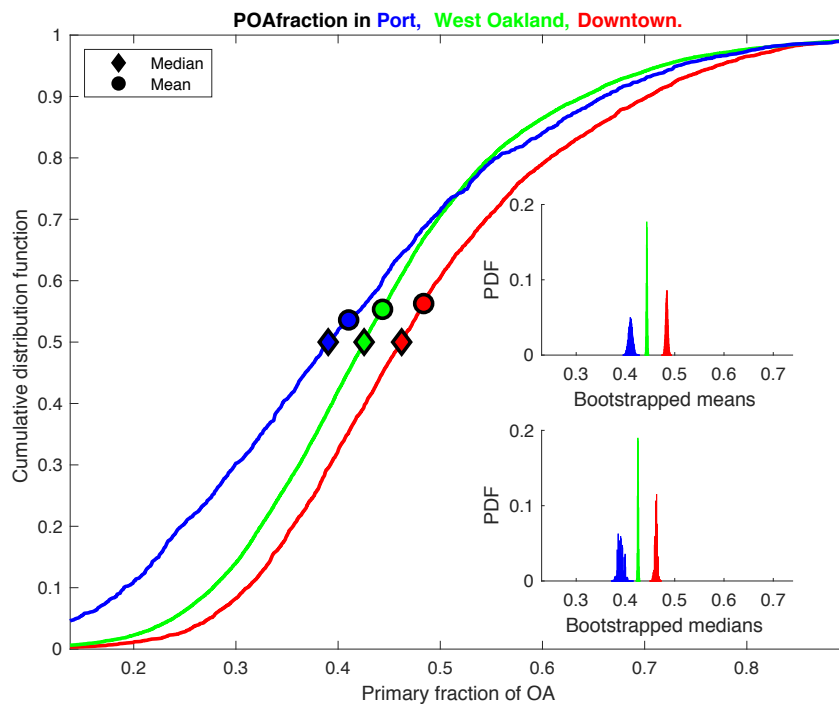


Figure S6. Cumulative distribution functions of primary fraction of OA (i.e., COA + HOA), resolved by area. Insets are results of bootstrapping.

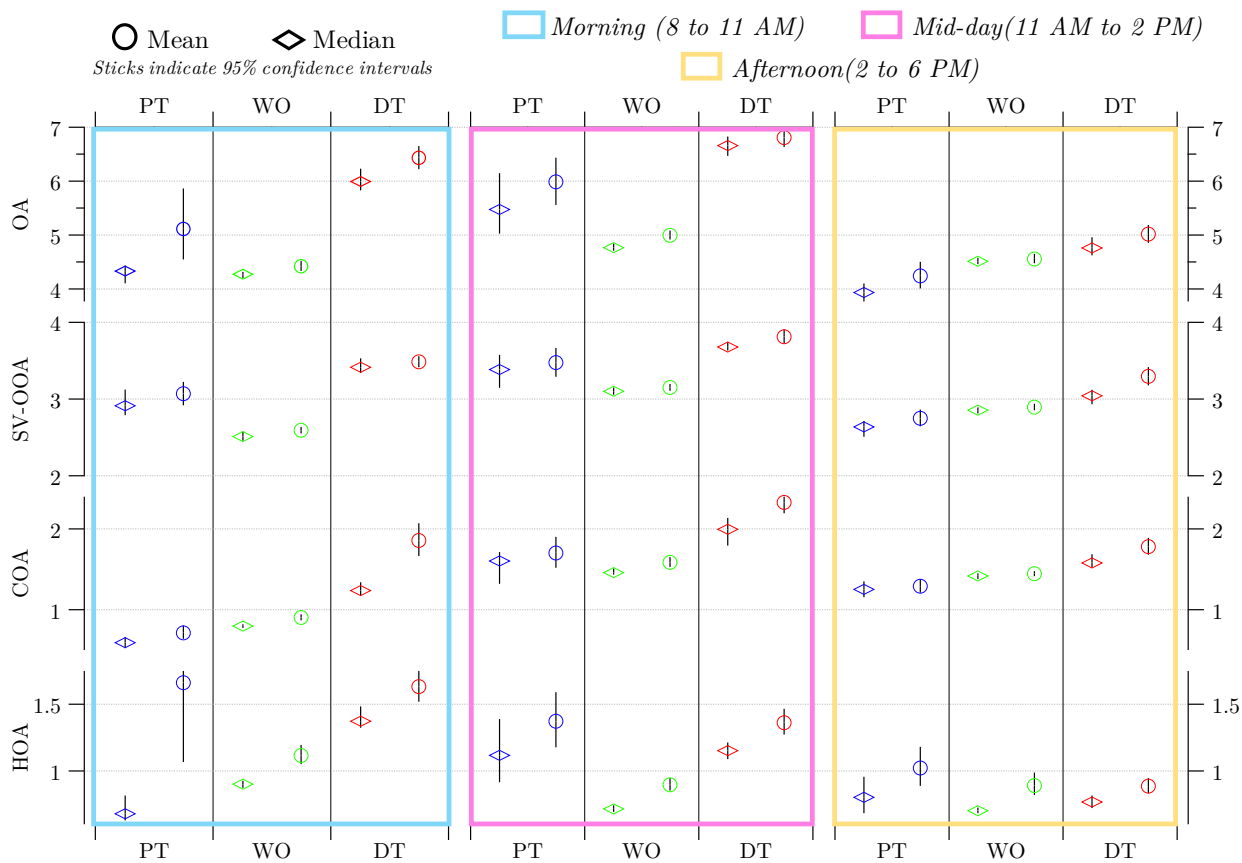


Figure S7. Bootstrapped statistics of OA and its factors, resolved by area and by time periods.

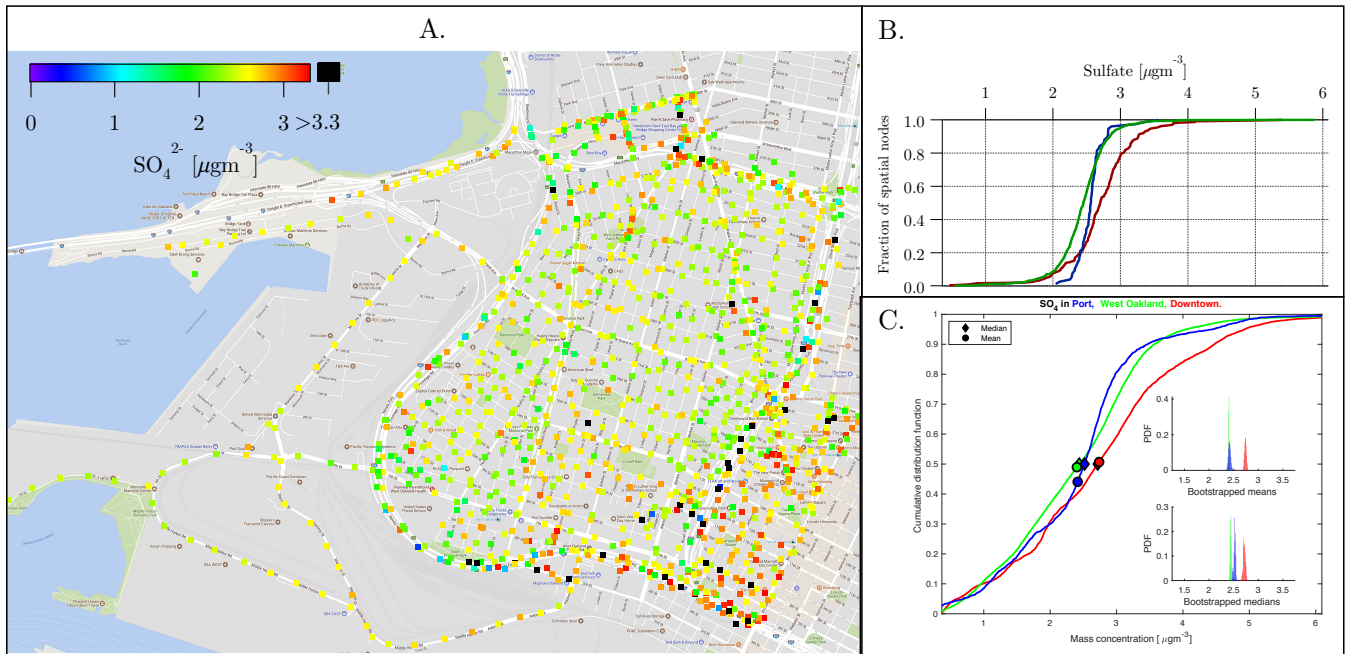


Figure S8. A: Median SO_4^{2-} at all magnets. **B:** Cumulative distribution function (CDF) curves of spatially-aggregated SO_4^{2-} concentrations. **C:** CDF curves of SO_4^{2-} concentrations without spatial aggregation. *Insets:* Probability distribution function (PDF) histograms for central tendency statistics (mean and median) of synthetic datasets created using bootstrap resampling of raw data. The abscissae on the insets have the same units as the parent abscissa, but with a zoomed-in scale.

It is seen that the CDFs of all polygons become “tighter” after spatial aggregation, which is expected, since the spatial aggregation routine reduces the spread in measurements via data reduction. However, the evidence of downtown being having a higher median (and especially higher mean) SO_4^{2-} than Port and West Oakland is not diminished by this data reduction, confirming that this trend is consistent across all days of sampling. Further, the SO_4^{2-} data exhibit minor positive skewness, suggesting that there are no local point sources of SO_4^{2-} in the domain.

A3 Quality of PMF solution

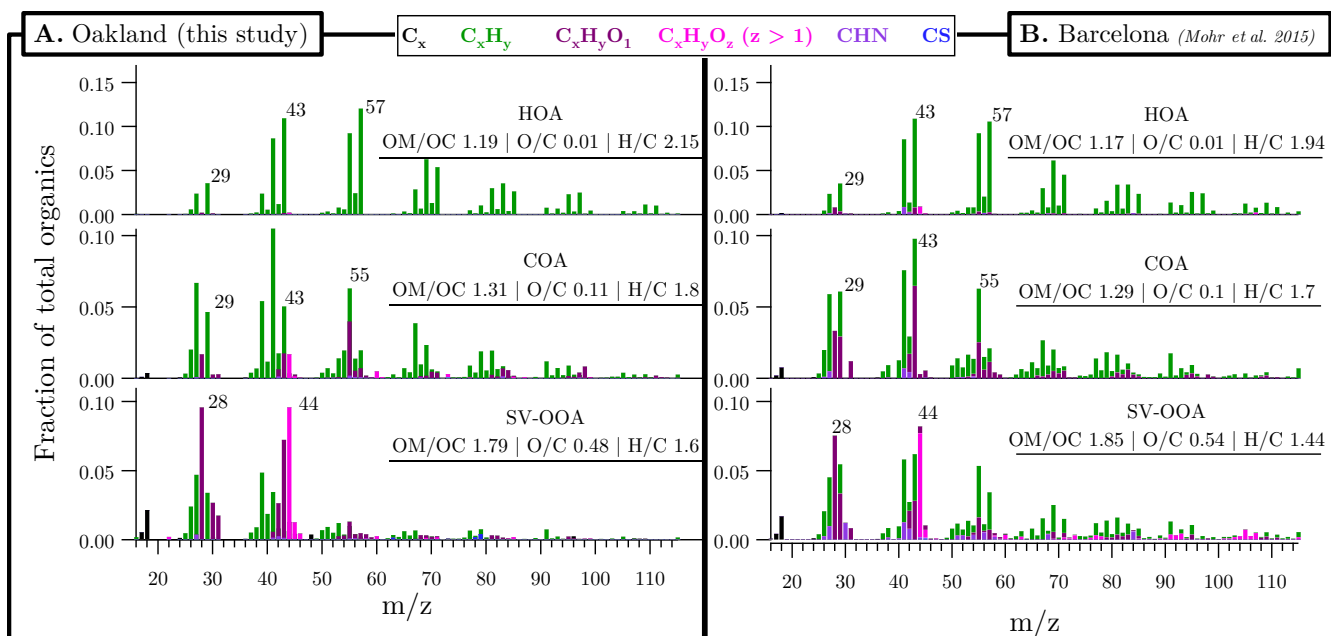


Figure S9. PMF factor mass spectra identified in **A.** Oakland and **B.** Barcelona (Mohr et al., 2015). Barcelona spectra obtained from the online high-resolution spectral database (Ulbrich et al., 2018, 2009).

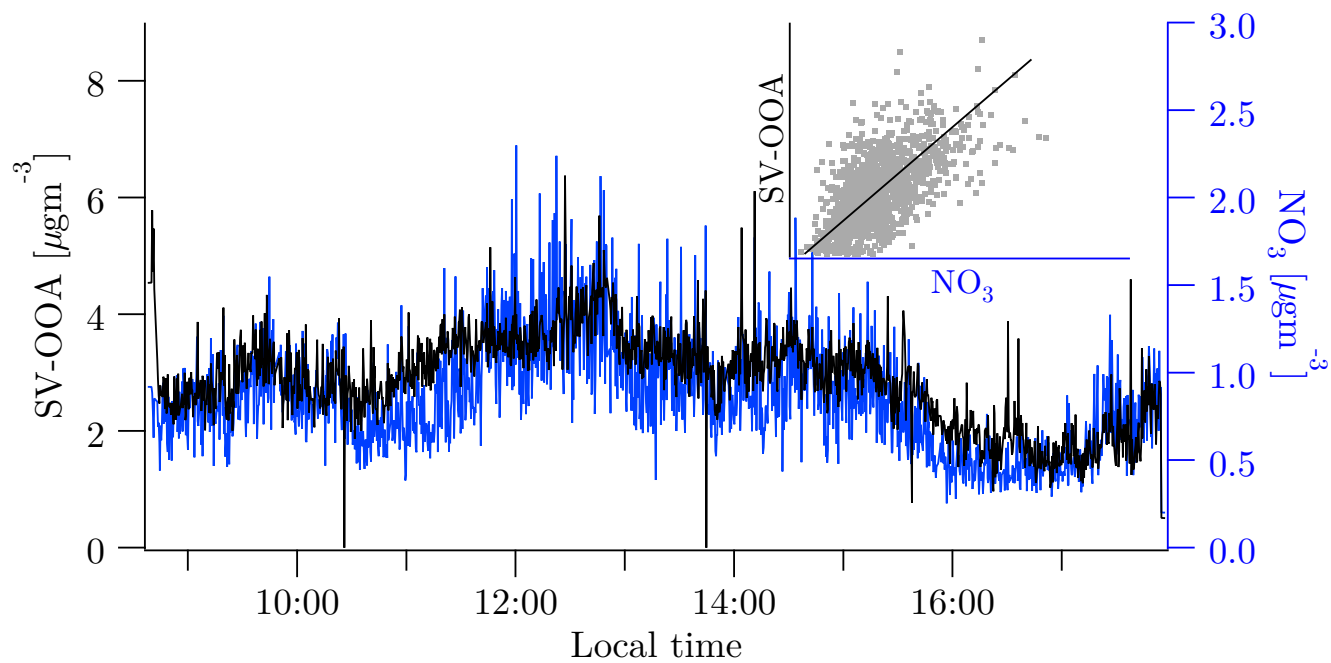


Figure S10. SV-OOA factor time series matched against NO₃⁻, a marker for semi-volatile photochemically aged OA.

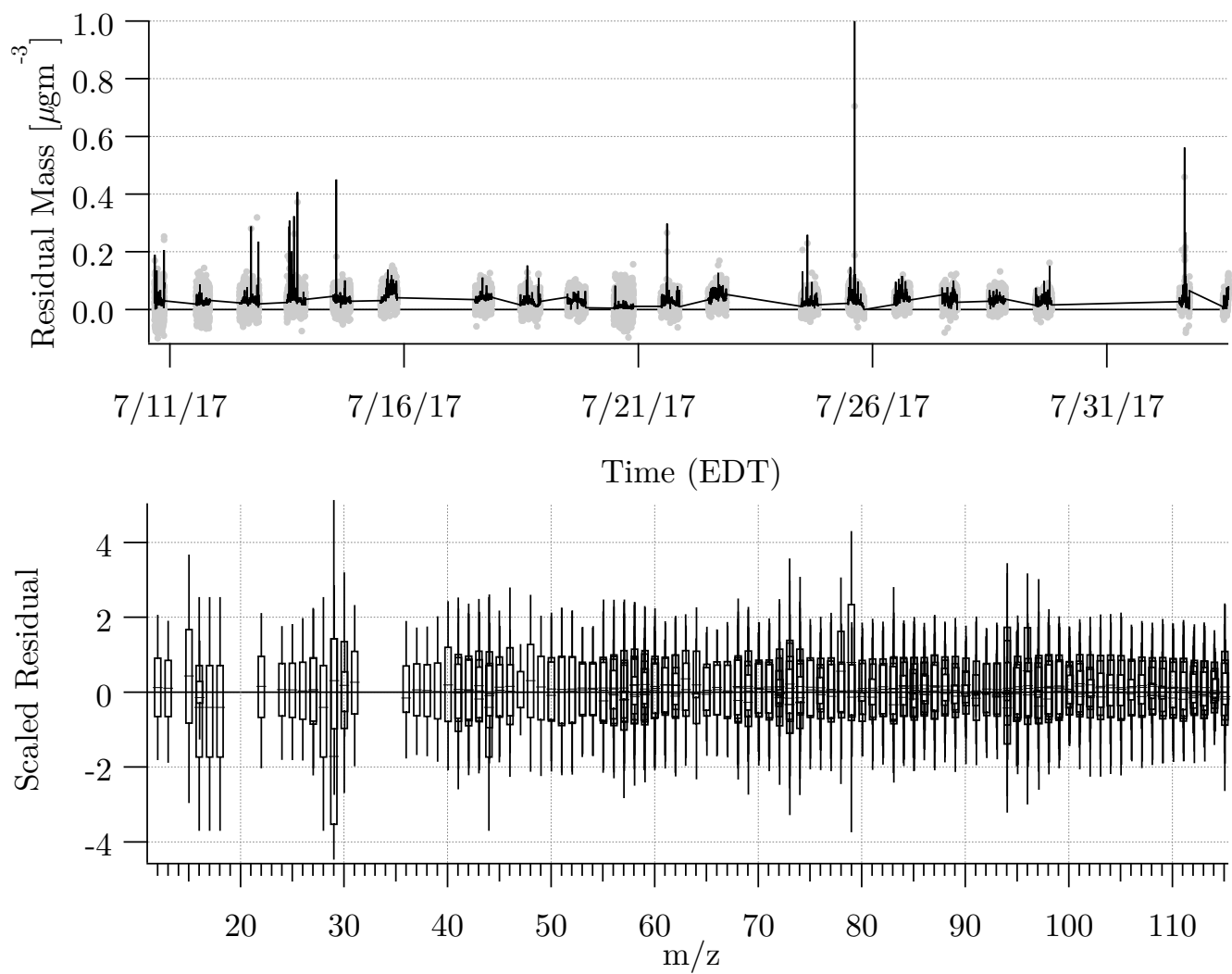


Figure S11. Residuals of three-factor PMF solution. The boxplots show the median (centerline) and quartiles (box limits) of the scaled residuals.

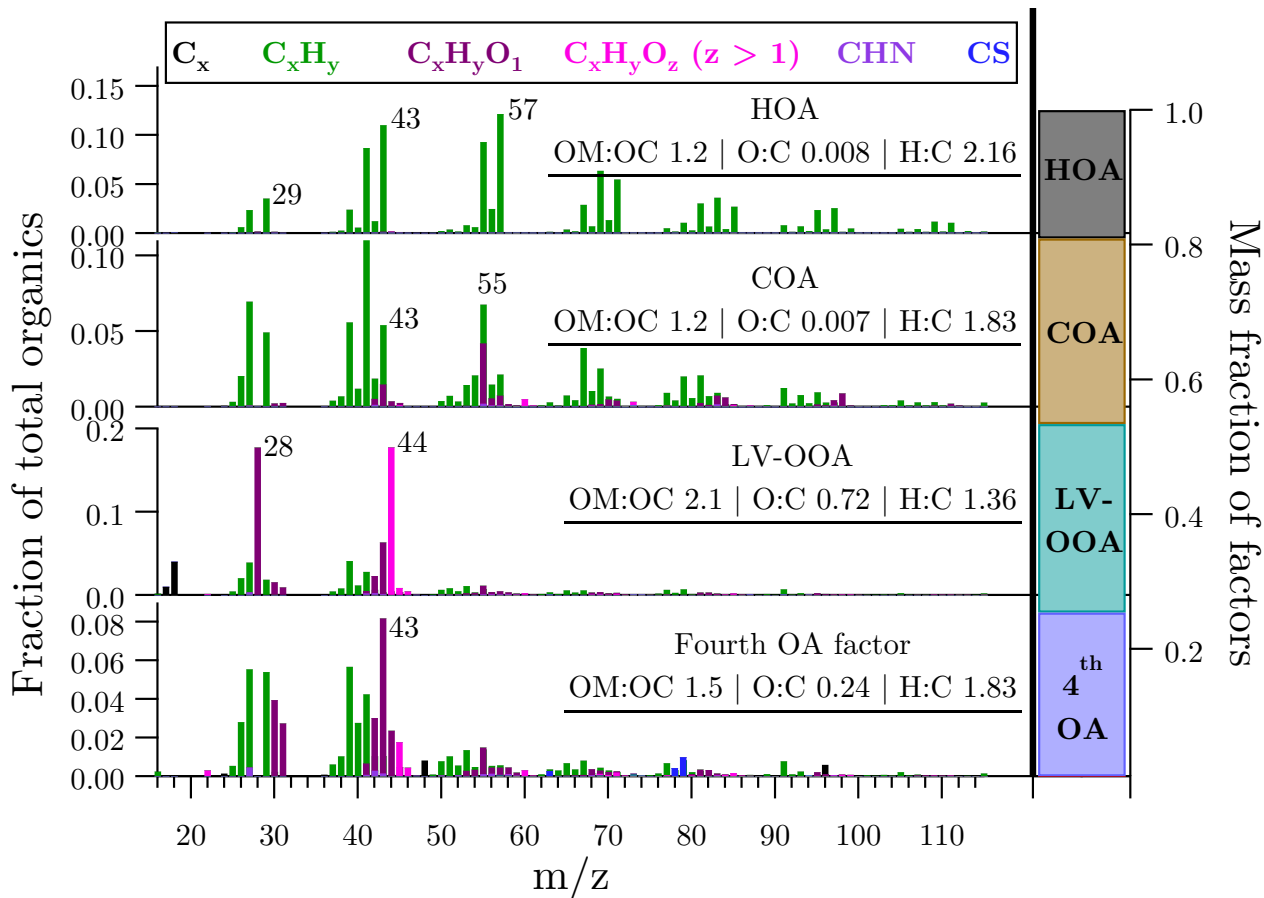


Figure S12. Mass spectra and elemental ratios of the four factors obtained from PMF analysis

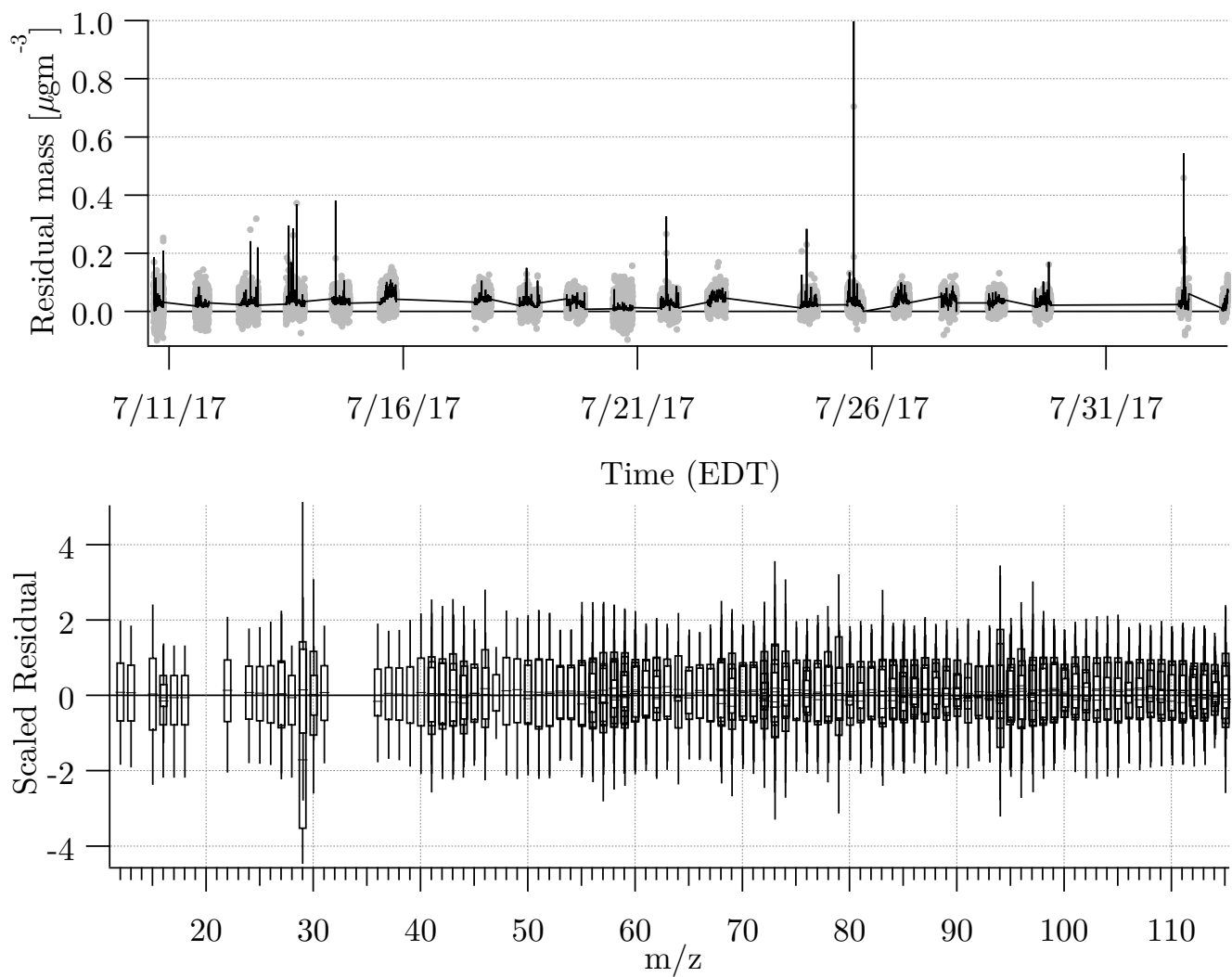


Figure S13. Residuals of four-factor PMF solution. The boxplots show the median (centerline) and quartiles (box limits) of the scaled residuals.

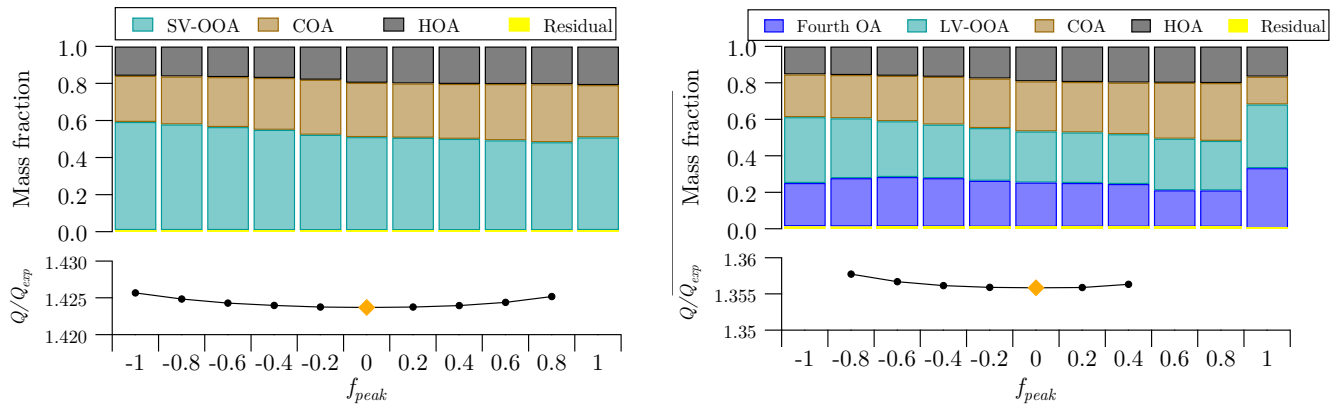


Figure S14. Variation in Q/Q_{exp} and mass fractions of factors with f_{peak} for 3- and 4-factor solutions. Q = sum of square of scaled residuals. Q_{exp} = number of degrees of freedom of the fitted data. Q/Q_{exp} should be ≈ 1 . f_{peak} is a rotational parameter that can be chosen to examine different possible variations within an n -factor solution (Ulbrich et al., 2009).

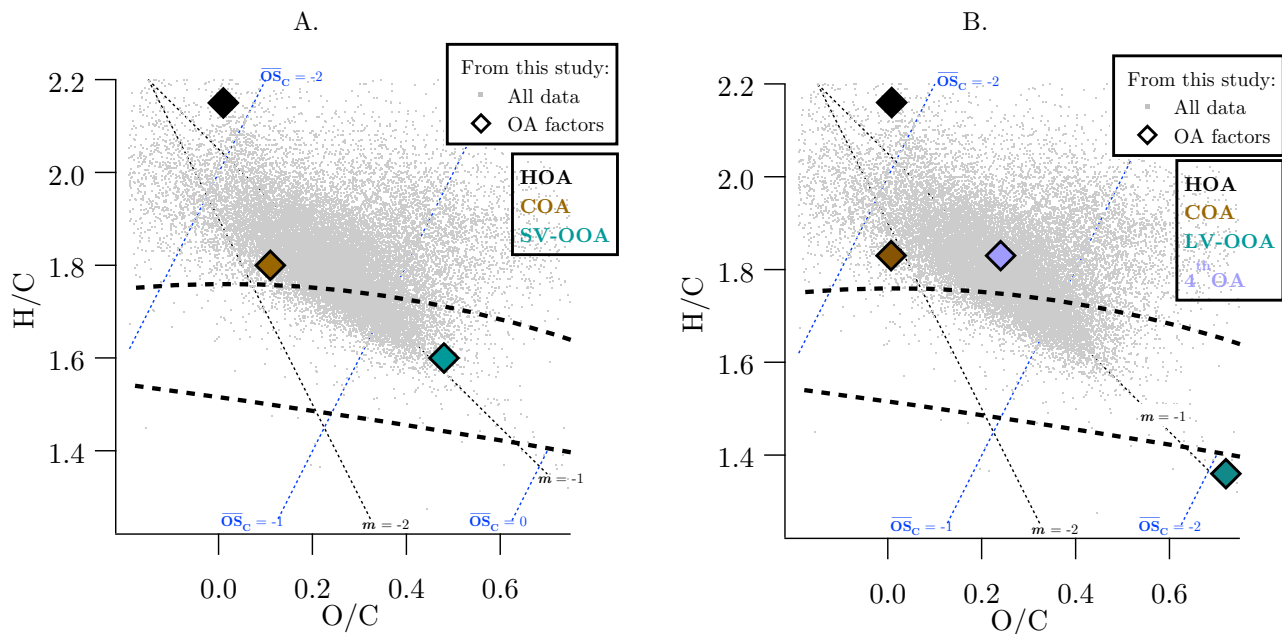


Figure S15. The Van Krevelen plane. Gray points represent all OA measurements in this study. Diamonds represent OA factors identified in the 3-factor (A.) and 4-factor (B.) PMF solution. Different oxygenation pathways are shown by the black dotted lines. Dotted blue lines are isopleths for average carbon oxidation states ($\overline{OS}_c = 2 \times O/C - H/C$). The region of ambient oxygenated OA measurements, as reported by Ng et al. (2011) is shown between the dashed curves.

A4 Wind measurements

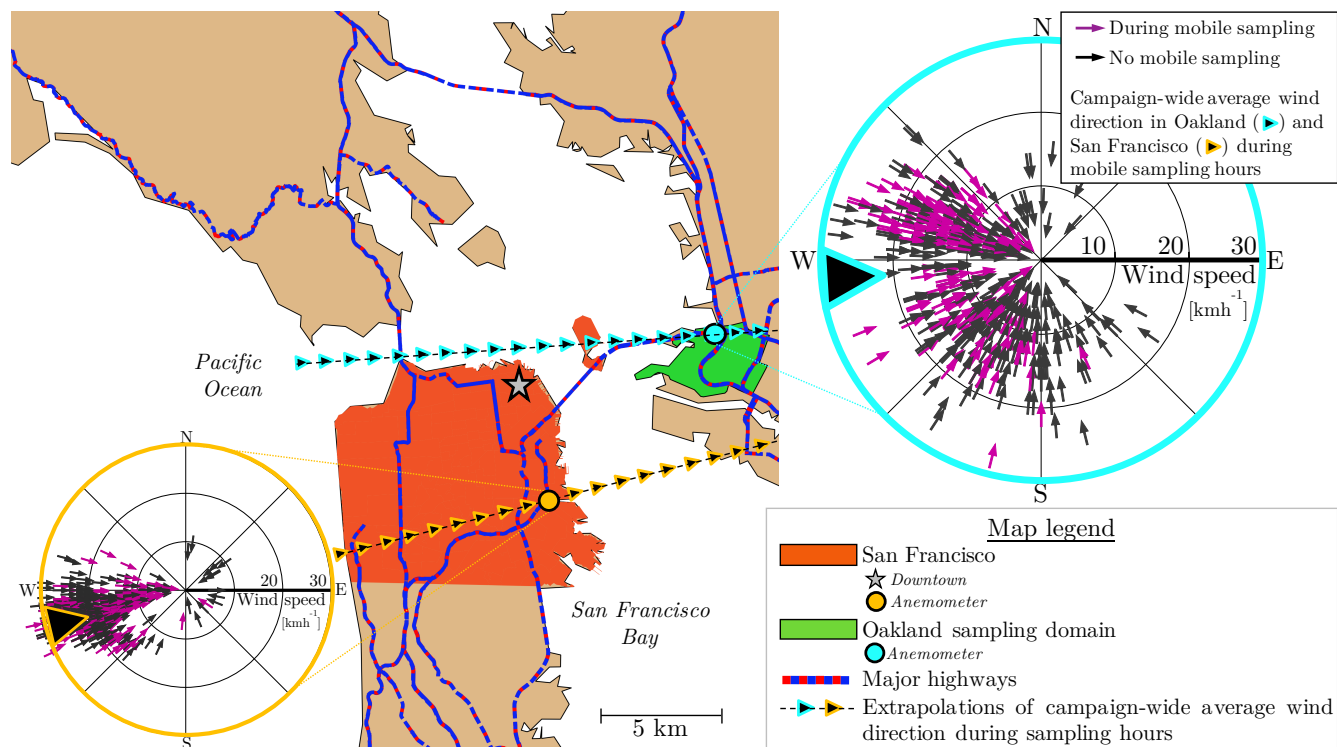


Figure S16. A map of the San Francisco (SF) Bay area, showing the location of the sampling domain in Oakland relative to SF city and downtown. Wind rose plots show hourly median wind speed and direction measured at two stationary anemometers in Oakland and San Francisco (BAAQMD, 2018). Purple wind rose arrows are wind measurements acquired during periods of concurrent mobile sampling (typically 8 am to 6 pm), while black arrows are measurements from when mobile sampling was not performed. A campaign-wide average of wind directions during periods of concurrent mobile sampling is shown by the triangle marker on each wind rose plot. The dashed lines with triangle markers are linear extrapolations of these campaign-wide average wind directions and are meant to guide the eye towards the regions over which these winds travel.

A5 OA factor maps

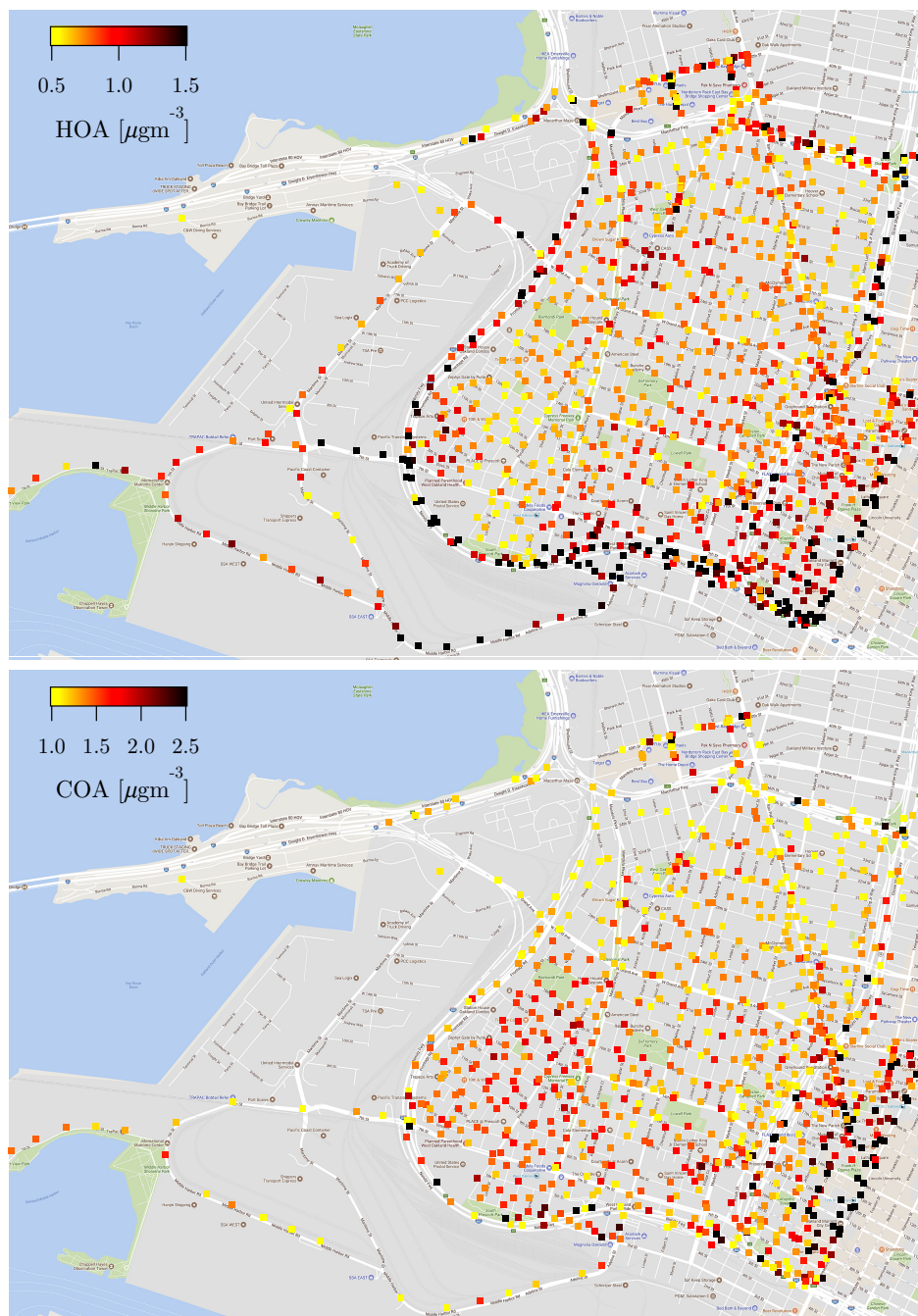


Figure S17. Maps of COA and HOA concentrations.

A6 Street canyon formation in downtown Oakland



Figure S18. Building height data for downtown polygon, obtained from City of Oakland (City of Oakland, 2017). The dashed black border shows limits of the downtown domain used in this study.